Investigation of the relationship between the spatial gradient of total electron content (TEC) and the occurrence of ionospheric irregularities

Teshome Dugassa[1,2], John Bosco Habarulema[3,4], and Melessew Nigussie[5]

[1]Ethiopian Space Science and Technology Institute, Department of Space Science and Application, Addis Ababa, Ethiopia
[2]Bule Hora University, College of Natural and Computational Science, Department of Physics, Bule Hora, Ethiopia
[3]South Africa National Space Agency, Space Science, Hermanus, South Africa
[4]Department of Physics and Electronics, Rhodes University, Grahamstown, South Africa
[5]Washera Geospace and Radar Science Laboratory, Physics Department, Bahir Dar University, Bahir Dar, Ethiopia

Correspondence: Teshome Dugassa (tdugassa2016@gmail.com), John Bosco Habarulema (jhabarulema@sansa.org.za), Melessew Nigussie (melessewnigussie@yahoo.com)

Abstract. The relation between the occurrence of ionospheric irregularity and the spatial gradient of total electron content (TEC) during the post-sunset hours over the equatorial region is investigated. Different instruments and techniques have been applied to study the behavior of these ionospheric irregularities. In this study, the Global Positioning System (GPS) based derived TEC was employed to investigate the relation between the spatial gradient of TEC between two nearby located stations and the occurrence of ionospheric irregularity over the East Africa longitudinal sector. The gradient of TEC between the two stations (ASAB: 4.34° N, 114.39° E and DEBK: 3.71° N, 109.34° E, geomagnetic) located within the equatorial region of Africa were considered in this study during the year 2014. The rate of change of TEC based derived index ($ROTI$, $ROTI_{ave}$) is also used to observe the relation between the spatial gradient of TEC and the occurrence of ionospheric irregularities over the stations. The result obtained shows that most of the maximum enhancement/reduction in the spatial gradient of TEC observed in March and September equinoxes are noticeable between 19:00 LT - 24:00 LT as the large-scale ionospheric irregularities do. Moreover, the observed spatial gradient of TEC shows two peaks (in March and September) and they exhibit equinoctial asymmetry where the March equinox is greater than September equinox. The maximum enhancement/reduction in the gradient of TEC and $ROTI_{ave}$ during the evening time period also show similar trends but after 1-2 hrs from the equatorial electric field (EEF). The relationship between the spatial gradient of TEC and ROTI observed during the nighttime hours correlate moderately with correlation coefficient of C = 0.58 and C = 0.53 over ASAB and DEBK, respectively. The vast majority of the spatial gradient of TEC are associated with ionospheric irregularities that occur during the evening period. In addition to latitudinal gradients, the spatial gradient of TEC has a significant contribution on the computation of TEC fluctuation. The spatial gradient of electron density (TEC) near solar-terminator obtained from two nearby located Global Navigation Satellite System (GNSS) receivers may be used as an alternative method to estimate the strength of the zonal electric field.

Key words: Spatial gradient of TEC, $ROTI_{ave}$, ionospheric irregularities

1 Introduction

The ionosphere, which consists of free electrons and ions, frequently experiences irregular electron density. After sunset, the ionospheric plasma interchange instabilities present in the equatorial/low-latitude ionosphere generate large-scale depletions in the ambient electron density which leads to the formation of plasma density irregularities that affect radio communication and navigation system (Basu and Basu, 1981). The generation of the plasma irregularities can be related to the decrease in plasma production immediately after sunset and the fast recombination rate in the E-region ionosphere, which results in a steep gradient in electron density. The large enhancement of F region vertical plasma drift in the evening hours which is due to the presence of enhanced eastward electric field was thought to control the generation of plasma density irregularities (Fejer, 1991; Fejer et al., 2008). This pre-reversal enhancement (PRE) in the vertical plasma drift moves the F region to higher altitudes (Abdu et al., 2009). When the altitude of F-region is high enough to overcome recombination effects, the Rayleigh-Taylor (R-T) instability mechanism initiates growth in plasma fluctuations. The R-T instability is considered primary responsible for the generation of ionospheric plasma density irregularities or plasma bubbles in equatorial and low-latitude region (Rao et al., 2006a; Fejer et al., 1999). Kelley (2009) reported that the existence of equatorial plasma bubbles (EPB) is attributed to the instability of the R-T plasma which is triggered by the intensification of the eastward equatorial electric field just before its reversal. The characteristics of ionospheric scintillation and ionospheric irregularities over the equatorial and low-latitude region in different longitudinal sectors during different solar and geomagnetic activities have been studied (e.g., Burke et al., 2004; Paznukhov et al., 2012; Oladipo and Schuler, 2013a; Seba and Tsegaye, 2015). From previous work, they have been studied by various instruments such as all-sky imager (Wiens et al., 2006), and very high-frequency radar observation (e.g., Otsuka et al., 2009; Ajith et al., 2016). Recently, Global Navigation Satellite System (GNSS) signal analysis is an important tool to study the behavior of ionospheric irregularities (e.g., Pi et al., 1997; Nishioka et al., 2008; Watthanasangmechai et al., 2016; Magdaleno et al., 2017) because of its growing application in civilian and military applications.

The inhomogeneity of ionospheric electron distribution can cause sudden, rapid and irregular fluctuations of the amplitude and phase of the received signals, known as ionospheric scintillation (Wernik and Liu, 1974). This inhomogeneity, i.e, spatial plasma density/TEC gradient, is higher at low-latitude region because of geomagnetic storms, equatorial spread F and Appleton ionospheric anomaly. As the GNSS signals pass through the ionosphere, the ionospheric irregularities also cause the delay of signals. The classification of the spatial electron density/TEC gradients can be given as latitudinal (north-south) and longitudinal (east-west) (Jakowski et al., 2004). It is normally found in the literature that the spatial plasma density gradients can be represented by means of TEC changes per latitude or longitude (TECU/deg) or by their changes in distance (TECU/km). In addition to causing an integrity treat for life-safety application to air traffic management (Rungraengwajiake et al., 2015), the ionospheric TEC gradient is also unfavorable for communication, and surveillance system which depends on trans-ionospheric signal propagation (Foster, 2000). Radicella et al. (2004) and Nava et al. (2007) also presented the contribution of the horizontal gradients of vertical TEC to positioning error. The characteristics of horizontal ionospheric density gradients and their effects on trans-ionospheric radio wave propagation have been studied at different latitudes (Jakowski et al., 2005; Radicella et al., 2004). It has been reported that the majority of large/steep gradient TEC gradients are associated with equatorial plasma

bubbles (Pradipta and Doherty, 2016). Rao et al. (2006a) estimated ionospheric spatial gradient from F-region peak electron density (NmF2) data using a chain of radio soundings. Based on the GNSS data acquired by dense distribution of receivers over Brazilian longitude sector, Cesaroni et al. (2015) highlights the relationship between intensity and variability of TEC gradients and the occurrence of ionospheric scintillation.

Previous studies attempt to explain the relation between the latitudinal (N-S) gradient of TEC surrounding the anomaly region and ionospheric scintillation over different sectors (Rao et al., 2006b; Ray et al., 2006; Muella et al., 2008). Recently, Seba et al. (2018) investigated the relation between equatorial ionization anomaly and night time equatorial spread F (ESF) over East Africa longitudinal sector using data from ground-based Global Positioning System (GPS) stations and a horizontal meridional neutral wind model. Even though, the characteristics of ionospheric irregularities/plasma bubbles over equatorial/low-latitude region of Africa under different solar and geomagnetic activities were discussed (Seba and Tsegaye, 2015; Seba and Nigussie, 2016; Mungufeni et al., 2016; Kassa and Damtie, 2017; Olwendo et al., 2018; Bolaji et al., 2019; Dugassa et al., 2019), a limited number of studies have been carried out over the region relating the latitudinal/longitudinal gradient of TEC/plasma density and the occurrence of ionospheric irregularities. To identify signals which severely suffer from ionospheric gradient, Ravi Chandra et al. (2009) and Rungraengwajiake et al. (2015) used rate of change of TEC (ROT) and rate of change of TEC index (ROTI). From the definition, however, ROTI mixes both the spatial and temporal gradients of TEC variations. The longitudinal gradient of integrated Pederson conductivity in the E-region at sunset time play a fundamental role in the strengthening the PRE magnitude and affect the generation of ionospheric irregularities (Tsunoda, 1985). It is well known that PRE is a postsunset phenomena which uplift the ionosphere and create a conducive condition for irregularity formation. This implies the magnitude of the zonal electric field is an important parameter for real-time prediction. It is also known that PRE is due to spatial gradient of electron density near solar-terminator. However, it is not easy to obtain the longitudinal gradient of electron density over Africa longitude sector as ionosondes are not available in nearby locations and study the relationship between the electron density gradient and occurrence of ionospheric irregularities. We know TEC is the integral of electron density, so a closely located GPS receivers would help us to estimate the strength of the zonal electric field and investigate the relation between the gradient of TEC and occurrence of irregularities. In this study, the relationship between the spatial gradient of TEC and occurrence of ionospheric irregularity were investigated using ground GPS-TEC receiver from two nearby located stations. The relation between the daytime eastward equatorial electric field derived from the equatorial electric field (EEF) model and the daytime equatorial electrojet (EEJ) obtained from ground based magnetometer measurements are also discussed. The study is the first of its kind in the African sector to present the relation between the spatial gradient of TEC and occurrence of ionospheric irregularities. The gradients of plasma density might be considered as an important parameter in the modeling of ionospheric irregularities and mitigating positioning errors on GNSS based application.

2 Data and analysis method

The GNSS data used for this study were obtained from University NAVSTAR Consortium (UNAVCO) database (http://www.unavco.org/). We used the data from two receiver stations located in the East African region at Debark (Geog. Lat. 13° N,

Geog. Long. 37.65° E, Geomag Lat. 4.13° N) and Asab (Geog. Lat. 13° N, Geog. Long. 42.65° E, Geomag. Lat. 4.85° N) for the period 2014. The receiver-independent exchange (RINEX) observation files obtained from the IGS website were processed by the GPS-TEC application software developed at Boston College (Seemala and Valladares, 2011; Ma and Maruyama, 2003). The TEC analysis software uses the phase and code values for both L1 and L2 GPS frequencies to eliminate the effect of clock errors and tropospheric water vapor to calculate relative values of slant TEC (Sardón and Zarraoa, 1997; Arikan et al., 2008). In order to avoid the multipath effects, different authors have used observation data above certain cutoff mask ranging from 15° to 35° (Chu et al., 2005; Mushini and Pokhotelov, 2011). In the current study, an elevation cutoff mask of 30° was used for all the VTEC computed.

There are two independent ways of estimating the TEC gradient values using ground based GPS receiver data (e.g., Lee et al., 2007, 2010). The first method uses a pair of closely-spaced receiver stations, looking at the same GPS satellite to calculate the difference in TEC values between the two neighboring ionospheric piercing points (IPP) at any given time. The second method uses a single GPS receiver station to infer the spatial TEC gradient values based on the observed temporal rate of change in TEC. Using the computed VTEC determined from the two receiver stations, the spatial gradient of TEC (difference of TEC between two stations per longitudinal separation) was computed for every time and then we analyzed its diurnal, monthly and seasonal variations. The two stations are located nearly along the same geographic latitude with longitudinal separation of about $\sim 5^\circ$ or corresponding spatial separation of 535.7 km. Stations with the same latitude were selected to observe only the contribution of the longitudinal gradient to TEC to the probability of occurrence of ionospheric irregularities expressed by ROTI. Vertical TEC (VTEC) values obtained by averaging the VTEC over 30 min intervals for a satellite and then averaged over all satellites in view are used in the computation of the gradient of TEC. The spatial gradient of TEC were computed using Eq. (1) (Lee et al., 2007; Ravi Chandra et al., 2009; Cesaroni et al., 2015).

$$Spatial\ gradient\ of\ TEC(t) = \frac{VTEC_{asab}(t) - VTEC_{debk}(t)}{\Delta lon} \tag{1}$$

where Δlon represents the difference in the longitude between the two stations. In the analysis of spatial gradient of TEC between the two stations, we applied the absolute value of TEC gradient. Radicella et al. (2004) used the absolute value of gradient of TEC between two stations to explain the effect of horizontal gradient of plasma density to ionospheric delay.

The time variation of TEC also known as rate of change of TEC (ROT) and its derived indices are a good proxy for the phase fluctuation, which is a measure of large-scale ionospheric irregularities (Aarons et al., 1997) used in this study. These kinds of indices can be used to characterize all the known features of equatorial spread F (ESF) (Mendillo et al., 2000). The rate of change of TEC (ROT) is given by

$$ROT = \frac{TEC_k^i - TEC_{k-1}^i}{t_k^i - t_{k-1}^i} \tag{2}$$

where i is the visible satellite and k is the time of epoch and ROT is in units of TECU/min. The ROTI is defined as the standard deviation of ROT over a 5-min period and mathematically given by Eq. (3) (Pi et al., 1997; Bhattacharyya et al., 2000;

Nishioka et al., 2008). Usually, ROTI > 0.5 TECU/min indicates the presence of ionospheric irregularities at scale lengths of a few kilometers (Ma and Maruyama, 2006).

$$ROTI = \sqrt{\langle ROT^2 \rangle - \langle ROT \rangle^2} \tag{3}$$

Oladipo and Schuler (2013b) employed the idea of Mendillo et al. (2000) to obtain a new index called $ROTI_{ave}$ index given in Eq. (4). $ROTI_{ave}$ index is the average of ROTI over 30 min interval for a satellite and then averaged over all satellites in view. The index gives average level of irregularities over half an hour. Recently, $ROTI_{ave}$ has been applied to demonstrate and explain the level of ionospheric irregularities over low-latitude/equatorial region of Africa (Oladipo et al., 2014; Bolaji et al., 2019; Dugassa et al., 2019). In this study, the rate TEC fluctuation index (ROTI) and ($ROTI_{ave}$) (Pi et al., 1997; Oladipo and Schuler, 2013b; Oladipo et al., 2014) were used to observe the occurrence of ionospheric irregularities.

$$ROTI_{ave}(0.5hr) = \frac{1}{N}\sum_{n=1}^{N}\sum_{i=1}^{k}\frac{ROTI(n, 0.5hr, i)}{k} \tag{4}$$

where n is the satellite number, $0.5hr$ is half an hour (0, 0.5, 1,... 23.5, 24 UT), i is the 5 min section within half an hour (i = 1, 2, 3, 4, 5, 6), N is the number of satellites observed within half an hour and k is the number of $ROTI$ values available within half an hour for a particular satellite. According to Oladipo and Schuler (2013b), the value of $ROTI_{ave} < 0.4$, $0.4 < ROTI_{ave} < 0.8$ and $ROTI_{ave} > 0.8$, respectively represents the background fluctuation, existence of phase fluctuation, and severe phase fluctuation activities. These threshold values were used to observe the relation between the occurrence of ionospheric irregularities and the spatial gradient of TEC.

The magnetic data used in this study are obtained from International Real-Time Magnetic Observatory Network (INTERMAGNET) and Africa-Meridian B-field Edication and Research (AMBER) installed in Addis Ababa (AAE, 9.0° N, 38.8° E, 0.2° N, geomagnetic) and Adigrat (ETHI, 14.3° N, 39.5° E, 6.0° N, geomagnetic), respectively. It provides one minute values of the northward (X), eastward (Y), vertical (Z) components of the Earth's magnetic field, from where the horizontal component (H) is computed using Eq. (5).

$$H = \sqrt{X^2 + Y^2} \tag{5}$$

To avoid different offset values of different magnetometers, the nighttime baseline values in the H component (Eq. 6) are first obtained for each day and subtracted from the corresponding magnetometer data sets and obtain the hourly departure of H denoted ΔH expressed by Eq. (7). The baseline value was defined as the average of the H component night time (23:00 - 02:00 LT) value of the Earth's magnetic field.

$$H_o = \frac{H_{23} + H_{24} + H_{01} + H_{02}}{4} \tag{6}$$

where H_{23}, H_{24}, H_{01}, and H_{02} are respectively the hourly values of H at 23:00, 24:00, 01:00 and 02:00 in local time (LT).

$$\Delta H(t) = H(t) - H_o \tag{7}$$

where t is the time in hours ranging from 01:00 to 24:00 LT. The hourly departure ΔH is then corrected for the non-cyclic variation (Eq. 8). This correction was proposed previously by Rastogi et al. (2004) who defined non-cyclic variation as a phenomenon in which the value at 01:00 LT is different from that of local midnight (24:00 LT).

$$\Delta c = \frac{\Delta H_{01} - \Delta H_{24}}{23} \tag{8}$$

The hourly departure of H (ΔH) corrected for the non-cyclic variation corresponding to magnetometer data set gives the solar quiet variation (Sq) values as shown in Eq. (9):

$$Sq(t) = \Delta H(t) + (t-1) * \Delta c \tag{9}$$

where t = 1 to 1440. The equatorial electrojet current (EEJ) produces a strong enhancement in the H-component magnetic field measured by magnetometers located within $\pm 5^\circ$ of the magnetic equator. Measurements of this magnetic field perturbation in equatorial magnetometers could provide a direct measure of the daytime equatorial electrojet (EEJ) and have strong relationships with dayside vertical velocity ($\boldsymbol{E} \times \boldsymbol{B}$ drift) (Anderson et al., 2004, 2006; Yizengaw et al., 2012). The equatorial stations respond primarily to the EEJ and also to the ring current and the global quiet time Sq current system. However, ground magnetometers just outside the extent of the EEJ ($\sim 6^\circ - 9^\circ$, off the dip equator) exhibit exact response to the ring and Sq currents, but near-zero response to the EEJ. To obtain the contribution of H-component field to the EEJ current (Eq. 10), we subtract the H-component value recorded at the off the equator ($\sim 6^\circ - 9^\circ$ geomagnetic) magnetometer from the H-component value measured at the magnetic equator. The subtraction has been made to remove the contribution of the ring current and global Sq dynamo to the H-component. Table 1 gives the list of all the stations for which data has been used in this study.

$$\Delta H = \Delta H_{AAE} - \Delta H_{ETHI} \tag{10}$$

The other data source used in this study is the Real-time model of the Ionospheric Electric Fields (http://geomag.org/models/PPEFM/RealtimeEF.html). The Prompt Penetration Electric Field Model (PPEFM) (Manoj and Maus, 2012) is a transfer function model which models the daily variations coming from the solar wind, which are mapped in the interplanetary electric field (IEF) data. Eight years IEF data from the ACE satellite, radar data from JULIA, and magnetometer data from the CHAMP satellite were used to derive the transfer function. Using the real-time data from ACE satellite, the transfer function models the current variations in the equatorial ionospheric electric fields. The model takes time and location as input parameters and

Table 1. Location information and the type of data used in this study.

Name of stations	Code	Geo. lon	Geo. lat	Geom. lon	Geom. lat	Data
Asab, Eritrea	ASAB	42.65° E	13° N	114.34° E	4.85° N	GPS-TEC
Debark, Ethiopia	DEBK	37.65° E	13° N	109.24° E	4.13° N	GPS-TEC
Addis Ababa, Ethiopia	AAE	38.77° E	9.04° N	110.47° E	0.18° N	Magnetometer
Adigrat, Ethiopia	ETHI	39.46° E	14.28° N	111.06° E	5.80° N	Magnetometer

calculates the best estimates of the equatorial electric field. The model outputs provide the electric field generated as a result of the convective electric field, quiet time electric field, and both. In the present study, we have used only the background quiet-time electric field to observe the relation between the equatorial electric field (EEF) and the spatial gradient of TEC derived from the two nearby stations.

Recently, Nayak et al. (2017) used the real-time model of an electric field to observe the influence of prompt penetration electric field (PPEF) on the occurrence of ionospheric irregularities during 17 March 2015 geomagnetic storm over Indian and Taiwan longitudes. However, this model has not been applied yet to explain the electrodynamic phenomena over African low-latitude region. To use the model in this region, we should first present its relation with equatorial electrojet (EEJ), an indicator of the eastward electric field, during the daytime period over the equatorial region of Africa. To do this, ground-based magnetometer measurements one located at magnetic equator and another one at ($\sim 6^\circ - 9^\circ$) off-equator (Rastogi and Klobuchar, 1990; Anderson et al., 2002; Yizengaw et al., 2014) have been used. Over East Africa longitude, two magnetometer stations, one at Adigrat (ETHI, 14.3° N, 39.5° E, 6.0° N, geomagnetic) and the other at Addis Ababa (AAE, 9.0° N, 38.8° E, 0.2° N, geomagnetic) exist. ETHI and AAE stations belong to AMBER network (Yizengaw and Moldwin, 2009) and INTERMAGNET, respectively. It has been reported that the strength of EEJ before sunset has a correlation with the generation of ESF during nighttime period preceded by rise in the F-region (Dabas et al., 2003; Uemoto et al., 2010; Ram et al., 2007). The relation between the EEF obtained from the real-time electric field model and ΔH were determined. EEF derived from the real-time electric field were used in this study to explain its influence on nighttime variations of the spatial gradient of TEC and the occurrence of ionospheric irregularities. The temporal resolution of EEF and ΔH was 5 min and 1 min, respectively. To make their resolution consistent, 5 min average of ΔH of each day were considered. In this study, ΔH derived from the horizontal (H) component of the geomagnetic field of the two stations during quiet days of the year 2012 were used. In this year, we have a large number of magnetometer measurements relative to other years. Monthly five quiet international days of the year 2012 (total of 38) obtained from (http://wdc.kugi.kyoto-u.ac.jp/qddays/index.html) were selected to show the correlation between ΔH and EEF. Since the EEJ is a day time phenomenon, only the daytime values of EEF and ΔH during (07:00 to 17:00 LT) were considered.

3 Results and Discussions

3.1 Relation between the day-time Equatorial Electrojet (EEJ) and Equatorial Electric Field Model (EEFM)

Figure 1a presents the diurnal variation of EEF and EEJ current signature of H-component of magnetic field on 26 March 2012. The correlation between the daytime EEJ derived from ΔH and EEF obtained from equatorial electric field model was shown in Figure. 1b. The ΔH and EEF show similar trend during the daytime period, 07:00 - 16:00 LT, as depicted in Figure 1a. To show the relation between ΔH and EEF, five (5) quiet international days of each month of year 2012 were selected. In the analysis, we considered the daytime (07:00 - 17:00 LT) value of ΔH and EEF. As illustrated in Figure 1b, during daytime (07:00 - 17:00 LT) period, the ΔH correlate positively and linearly with EEF with correlation coefficient, C = 0.60. Anderson et al. (2002) proposed ΔH deduced from ground-based magnetometers as a proxy of equatorial electrojet current. They reported that the vertical plasma drifts observed from Jicamarca incoherent scatter radar (ISR) has a positive and linear relation with ΔH and henceforth the ΔH was widely taken as a substitution for the EEF. Anderson et al. (2006) and Yizengaw et al. (2011) also reported a strong relation between the dayside vertical velocity ($\boldsymbol{E} \times \boldsymbol{B}$ drift) and ΔH. Studies show that the daytime electrodynamics play a decisive role in the initiation of post-sunset ESF (e.g., Mendillo et al., 2001; Valladares et al., 2001, 2004). The connection between the occurrence of ESF during the evening sector preceded by the rapid rise in F-layer and the strength of EEJ before sunset has been presented (Dabas et al., 2003; Burke et al., 2004; Kelley, 2009; Uemoto et al., 2010; Ram et al., 2007). Sreeja et al. (2009) reported observational evidence for the plausible linkage between the daytime EEJ related electric field variations with the postsunset F-region electrodynamics. Furthermore, Hajra et al. (2012) indicate that the afternoon/evening time variation of the eastward electric field as revealed through EEJ seems to play a dominant role in dictating postsunset resurgence of EIA and consequent generation of spread-F irregularities. Since the equatorial electric field derived model (EEF) correlate moderately with ΔH over East Africa longitudinal sector, we might use EEF model over equatorial/low-latitude region of Africa to explain some special features of ionospheric phenomena like plasma density irregularities and the positive/negative in the spatial gradient of TEC between the two stations.

3.2 Relation between the equatorial electric field (EEF), the spatial gradient of TEC and occurrence of ionospheric irregularities

Figure 2 (a-l) shows the diurnal variation of the quiet-monthly mean of spatial gradient of TEC (blue curves) in the year 2014. The quiet-monthly mean of EEF (along $\sim 40^{\circ}$ E) (red curves) were also over plotted with spatial gradient in TEC. We over plot both EEF and spatial gradient in TEC to observe the effect of EEF on the variability of the gradient in TEC and/or occurrence of ionospheric irregularities. In the computation of the spatial gradient of TEC (using Eq. 1), negative/positive values in the gradient of TEC may be observed during the nighttime or daytime. Both the negative and positive differences of TEC between the two stations show the gradient of TEC. It is obvious that positive/negative gradient in TEC is obtained when the minuend is larger/smaller than the subtrahend. A positive/negative gradient in TEC denotes an enhancement/reduction in TEC or electron density over ASAB relative to DEBK. This difference may be attributed to different physical processes, like neutral winds and plasma drift. In this study, the term maximum enhancement/reduction in the gradient of TEC (in terms of magnitude)

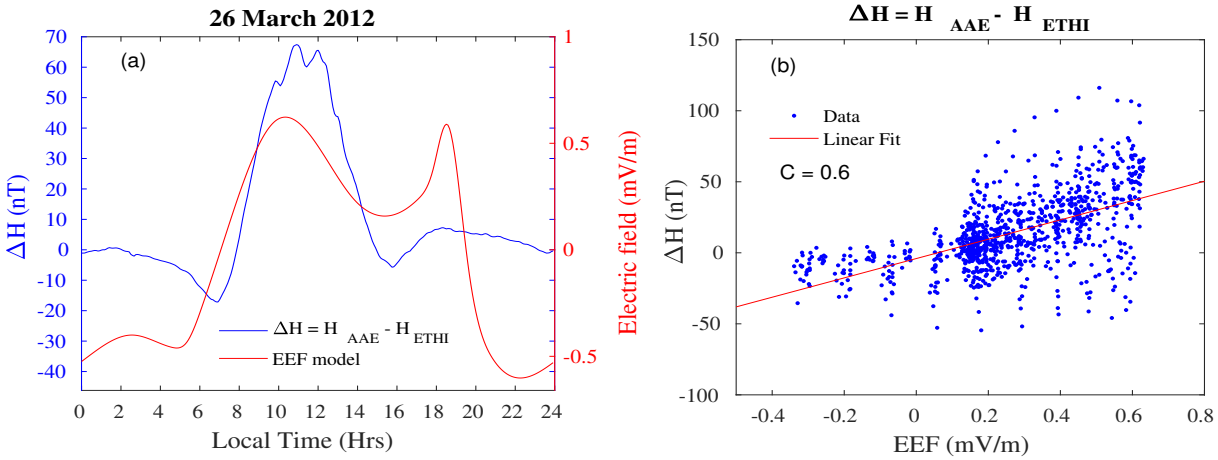

Figure 1. (a) Example showing the diurnal variation of Equatorial Electric field Model (EEF) (red curve) and ΔH (blue curve) during 26 March 2012 and (b) The correlation between the equatorial electrojet (EEJ) and quiet-time equatorial electric field model (EEF) during day-time (07:00-17:00 LT) period for quiet days of year 2012. The red line shows the linear fit of data points.

when the nighttime value of gradient of TEC was larger than the daytime value. There were also cases where the gradient in TEC during the daytime was greater than nigh time values. It can be seen from Figure 2 (red curves) that around evening hours, enhancement in EEF were observed in the equinoctial months and was relatively weak during the June and December solstices. It has been stated that an enhanced eastward electric field will be produced from the electrodynamical interaction of the eastward thermospheric wind with the geomagnetic field around the dip equator at the sunset terminator when longitudinal gradient conductivity exist between the high-conducting dayside ionosphere and the low-conducting nightside ionosphere (Batista et al., 1986; Heelis et al., 1974). Most of the enhancement/reduction in the TEC gradient was observed in the pre-midnight (19:00 - 24:00 LT) and postmidnight (24:00 - 06:00 LT) but after 1-2 hr of the post-sunset enhancement of the equatorial electric field. During the nighttime period, the maximum enhancement/reduction in spatial gradient of TEC found mostly in the range between -1.0 TECU/deg and 1.0 TECU/deg. A variation in the spatial gradient of TEC observed in the pre-midnight may be due to the plasma bubbles Ratnam et al. (2018). In some days, the spatial gradient of TEC observed during the daytime was relatively small compared to the evening time hours. The maximum enhancement/reduction in the gradient of TEC and the peak in the EEF observed during the pre-midnight period was significant during the equinoctial months. After post-sunset period, the maximum enhancement/reduction in the gradient of TEC in solstice months was small compared to equinoctial months, when PRE electric field observed in the evening period was minimum. Yoshihara et al. (2005) confirm the larger ionospheric gradients during summer and followed by autumn. The ionospheric gradients are less during winter as compared to summer and autumn. The enhancement/reduction in the gradient of TEC observed in the evening period may be related to the PRE in a zonal electric field.

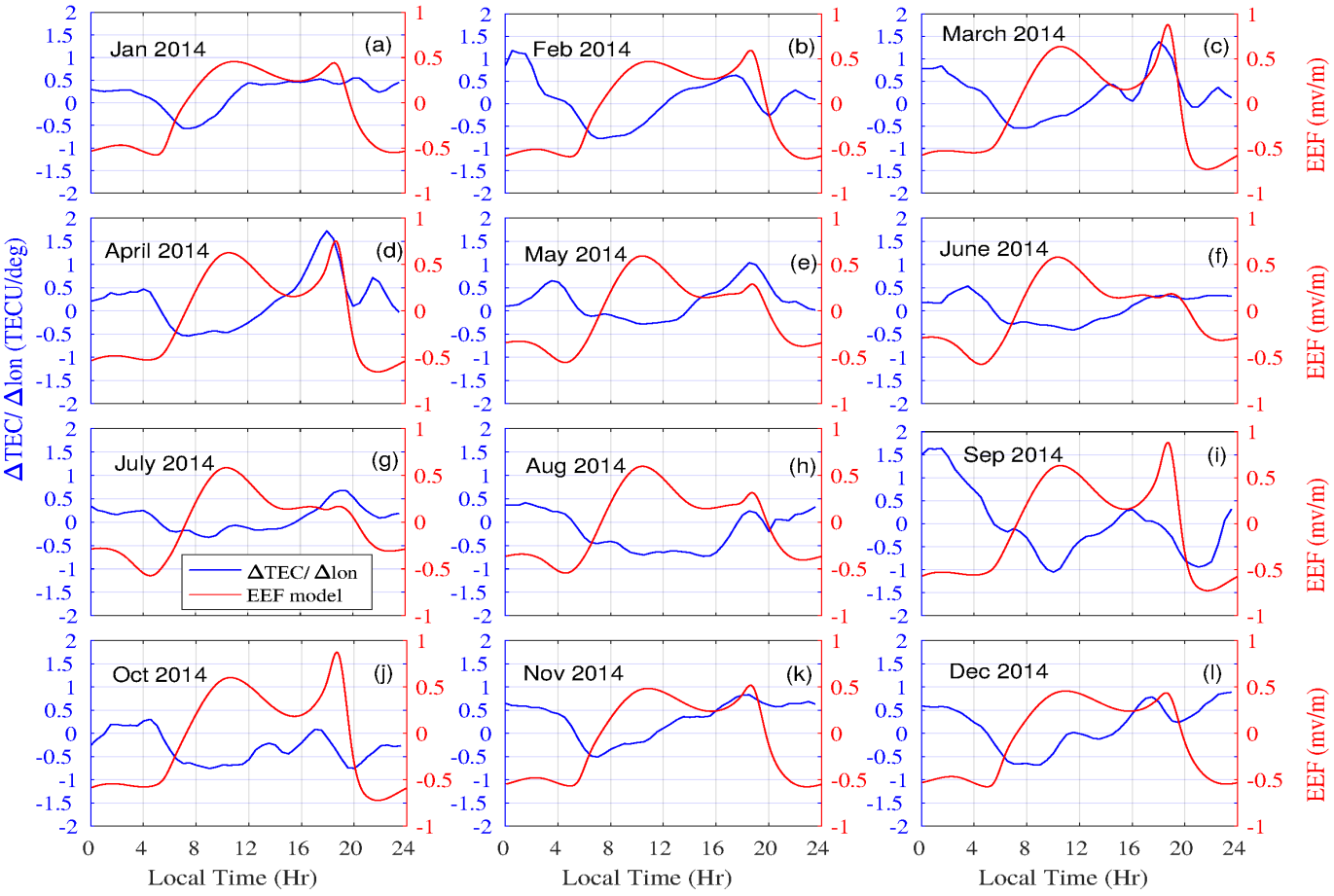

Figure 2. Comparison of Quiet-Monthly Mean of EEF derived from real-time electric field model at about ($\sim 40^{\circ}$ E) and spatial gradient of TEC between ASAB and DEBK in the year 2014.

Figures 3 (a - d) indicate representative cases showing the diurnal variations of the spatial gradient of TEC (blue curve) and ROTI (red and black curves) over ASAB and DEBK stations. The $ROTI_{ave}$ values in each panel was greater than 0.4 TECU/min, a threshold value showing the presence of irregularities in the premidnight hours. Likewise, maximum enhancement/reduction in the gradient of TEC were observed during pre-midnight and post-midnight periods. It is evident from Figure 3 during nighttime period (after 18:00 LT) that the pattern of ROTI (observed in both stations) and the spatial gradient in TEC show a kind of similar trend. Different researchers used the concept of ionosphere spatial gradient based on multi-GNSS observations within a small scale region to provide corrections and integrity information to the Ground-Based Augmentation System (GBAS) (Rungraengwajiake et al., 2015; Saito and Yoshihara, 2017). They attribute the large ionosphere spatial gradient to the TEC enhancements and the ionosphere irregularities. Saito and Yoshihara (2017) associated spatial gradient in ionospheric TEC with plasma bubbles. Sun et al. (2013) examined the relationship between the storm-enhanced plasma density (SED)-associated irregularities (ROTI) and TEC gradients over continental United States (CONUS) during the geomagnetic

storms. Rungraengwajiake et al. (2015) analyzed plasma bubbles at postsunset equinox time and observed the higher scales in east-west gradient compared with north-south gradients for GBAS system, however, Cesaroni et al. (2015) reported that north-south gradient in TEC correlates well with ionospheric scintillation than the east-west gradient of TEC. The plasma density variability, either the spatial and/or temporal, causes not only the GNSS-based positioning error but also radio wave scintillation.

The maximum enhancement/reduction in the gradient of TEC and the associated ionospheric irregularity during the post-sunset period could be explained by the presence of ionospheric electrodynamics. It is well known that Earth's equatorial ionosphere presents dynamically temporal and spatial variations. The electrodynamics of low-latitude ionosphere after sunset is influenced by F-region dynamo which is governed by a longitudinal gradient of the electrical conductivity and thermospheric zonal wind (Crain et al., 1993). Anderson et al. (2004) showed that the scintillation activity is related to the maximum $E \times B$ drift velocity between 18:30 LT and 19:00 LT. Mendillo et al. (2001) have pointed out that the best available precursor for pre-midnight equatorial spread F (ESF) is the equatorial ionization anomaly (EIA) strength at sunset, which is in turn influenced by the magnitude of PRE. Using differential TEC profiles, TEC (at 18:00 hr) - TEC (at 20:00 hr), Valladares et al. (2004) explained that the PRE of the vertical drift would re-energize the fountain effect. The postsunset EIA produces a large plasma density gradient from the trough region to th crest region. Takahashi et al. (2016) observed a most steep in TEC gradient with a difference of 30-50 TECU from the inside to outside plasma bubbles.

In the evening sectors, the vertical drift enhancement is of particular significance as it is the major drivers for the generation of ESF (Farley et al., 1970; Woodman, 1970; Basu et al., 1996; Fejer et al., 1999; Martinis et al., 2005). Tulasi Ram et al. (2006) reported that the rapid enhancement of post-sunset of the zonal electric field leads to a large vertical plasma drift ($\boldsymbol{E} \times \boldsymbol{B}$), thereby lifting the F-layer to higher altitudes resulting in a condition conducive for the generation of ESF. Ionospheric irregularities are mostly observed over equatorial/low-latitude region an hour or two hours after the PRE. Rastogi and Woodman (1978) showed ESF can appear at any time of the night other than the post-sunset period following the abnormal reversal of the vertical F-region drifts to an upward direction, with a delay of about 1-2 hr. As illustrated in Figure 2, the influence of post-sunset enhancement in the zonal electric field on the maximum enhancement/reduction in the spatial gradient of TEC during the post-sunset period can be seen. This may indicate the maximum enhancement/reduction in the spatial gradient of TEC and the occurrence of ionospheric irregularities have some degree of relationship.

Figures 4 (a-d) indicate representative cases for ROTI (red and black curves) and spatial gradient in TEC (blue curve) when the occurrence of ionospheric irregularities are absent. The value of $ROTI_{ave}$ was less than 0.4 TECU/min, showing non-occurrence of ionospheric irregularities. In these cases, the maximum enhancement/reduction in spatial gradient of TEC were observed during day and/or nighttime period. When the occurrence of irregularities are absent, an enhancement/reduction in the gradient of TEC in the postsunset period also observed (Figure 4 a). The pattern in the spatial gradient of TEC and ROTI during geomagnetic storm days were also illustrated in Fig.5 (a-d). These storm days are categorized as moderate magnetic storms (-100 nT $\leq$ Dst $\leq$-50 nT) (Loewe and Prölss, 1997; Echer et al., 2013). When the presence of ionospheric irregularities

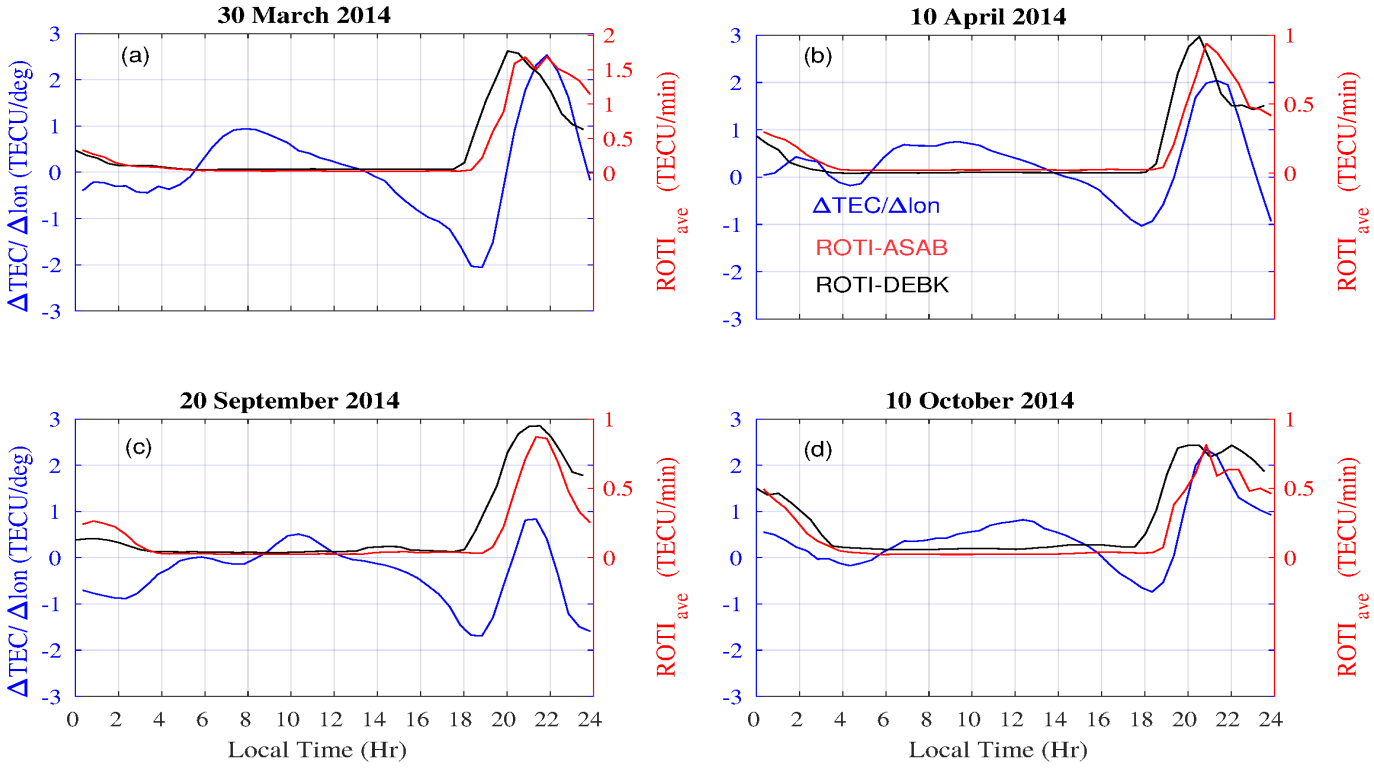

Figure 3. Typical examples of diurnal variation in the spatial gradient of TEC (blue curve) and the ROTI over ASAB (red curve) and DEBK (black curves) on a) 30 March 2014, b) 10 April 2014, c) 20 September 2014 and d) 10 October 2014.

are observed (ROTIave$\geq$ 0.4 TECU/min), the magnitude of spatial gradient of TEC in the post-sunset period is enhanced (during 13 September 2014) and when its presence suppressed (ROTIave$<$ 0.4 TECU/min), the magnitude of TEC gradient in the nighttime period is reduced (19 February and 27 August 2014). On those days, the spatial gradient in TEC observed during the daytime hours show maximum enhancement/reduction.

Figures 6a and b show ionospheric irregularity occurrence using the phase fluctuation index ($ROTI_{ave}$) at ASAB and DEBK in the year 2014, respectively. The $ROTI_{ave}$ values are indicated in the color bar. As stated by Oladipo and Schuler (2013b), the value of $ROTI_{ave} \geq 0.4$ shows the presence of ionospheric irregularity. The occurrence of ionospheric irregularities at the two stations, as indicated by intensity level of $ROTI_{ave}$, was predominantly observed in the premidnight periods, mainly between 19:00 LT and 24:00 LT. The large-scale ionospheric irregularities, which are responsible for the scintillation of trans-ionospheric signals at GNSS frequencies, are more pronounced during post-sunset hours. The observed phase fluctuation shows monthly variations and there is also a seasonal trend in the occurrence of ionospheric irregularity. Strong and weak ionospheric irregularities are observed in March equinox and in June/July solstices, respectively.

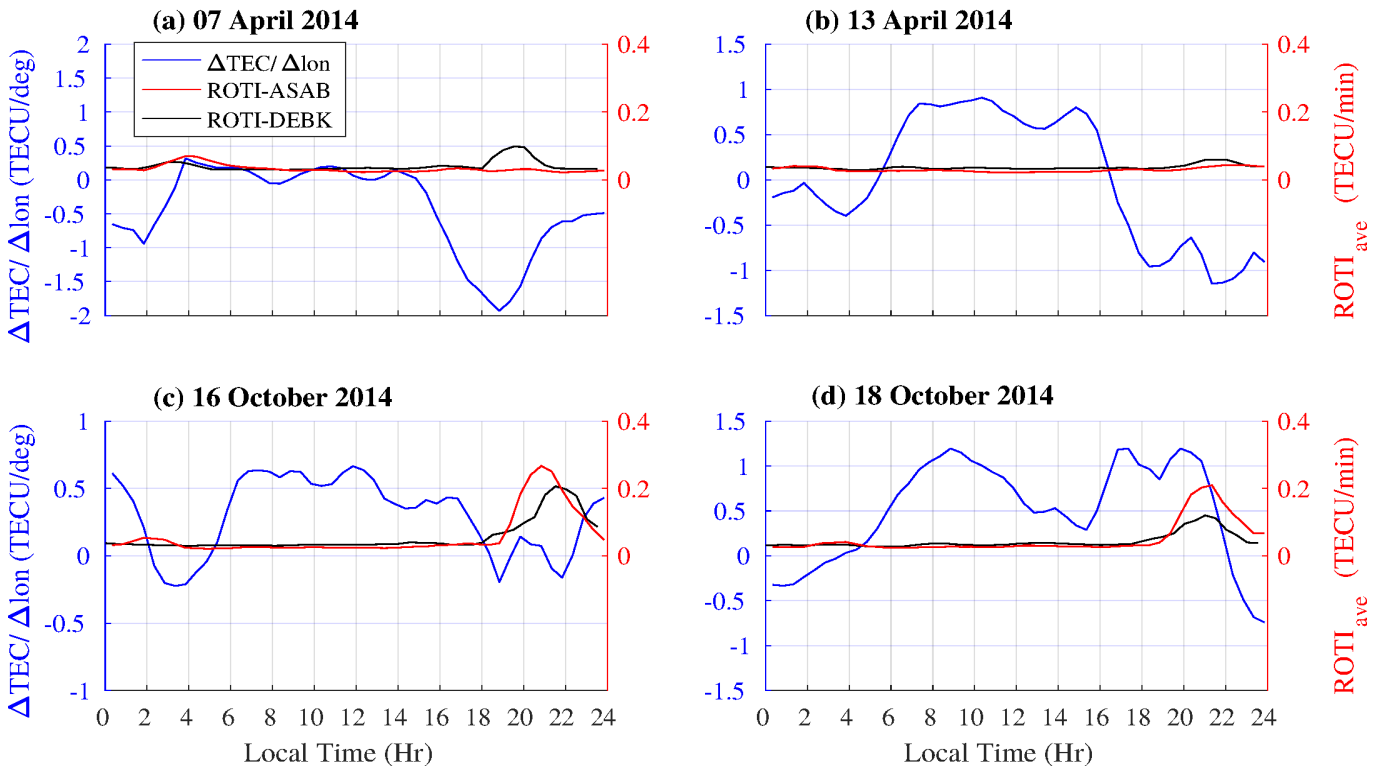

Figure 4. Examples showing the absence of ionospheric irregularities observed using ROTI and its relation with spatial gradient of TEC on (a) 12 April 2014 (b) 13 April 2014 (c) 16 October 2014 and (d) 18 October 2014.

Figure 6c shows the annual variation in the spatial gradient of TEC between DEBK and ASAB in the year 2014. The maximum enhancement/reduction in the value of the gradient of TEC were observed mostly during the post-sunset (18:00 - 24:00 LT) and postmidnight (24:00 - 06:00 LT) period. Equation (1) was applied to all days (364 days) of year 2014 in computing the spatial gradient of TEC. Out of the total observed daily maximum value of the gradient of TEC, about 194 days (in percent about 53 %) of them fall in this time period. There was also a case where the maximum enhancement and reduction in the value of the gradient of TEC were observed in the early morning period.

Figure 6c shows the daily maximum positive (blue dots) and maximum negative (red dots) in values of TEC gradient. The maximum enhancement/reduction in the gradient of TEC were mostly observed during post-sunset and postmidnight period. They also show monthly and seasonal variations. The maximum peak/reduced values of the spatial gradient of TEC observed in equinoctial months are greater than solstice months. Equinoctial asymmetry in the occurrence of TEC gradient was also noticed. TEC gradient in March equinox was greater than that in September equinox. The minimum values in the spatial gradient of TEC observed mostly during post-sunset and post-midnight periods show similar trend with that of the maximum enhancement. They also show an equinoctial asymmetry, where TEC gradient in March equinoxes were greater than the one obtained for September equinoxes.

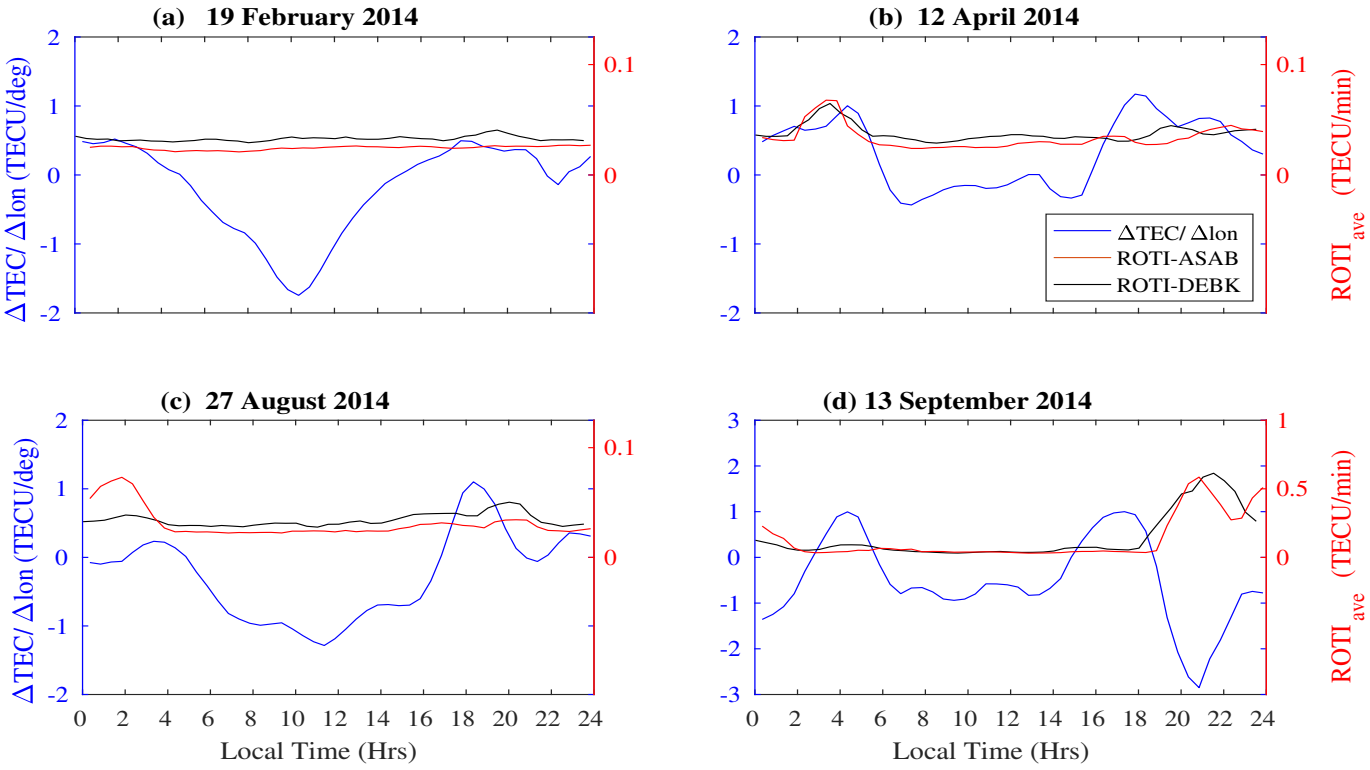

Figure 5. Representative examples showing diurnal variation of the patterns of the spatial gradient of TEC and the ROTI over ASAB and DEBK stations during geomagnetic storm days (a) 19 February 2014 (b) 12 April 2014 (c) 27 August 2014 and (d) 13 September 2014.

Figures 6d and e present the daily maximum values of the phase fluctuation index ($ROTI_{ave}$) over ASAB and DEBK stations, respectively and Fig. 6f shows the daily maximum and minimum value of the gradient of TEC in the year 2014. It is clearly observed from Figures 6 (d-f) that the enhancement in $ROTI_{ave}$ and gradient of TEC shows monthly and seasonal variations, and also equinoctial asymmetry is observed. The daily maximum value of the spatial gradient of TEC shows a kind of similar trends with the daily maximum value of $ROTI_{ave}$ observed over ASAB and DEBK stations. The trend they show has similarity with the time of occurrence of maximum enhancement, monthly and seasonal variations. Moreover, the seasonal variation observed in both variables exhibits equinoctial asymmetry, where the March equinox was greater than September equinoxes. The mechanism of generation of the enhancement in vertical drift just after sunset was detailed by Farley et al. (2008). The magnitude of peak vertical drift is known to control the seasonal and day-to-day variations in the occurrence of equatorial spread F (Manju et al., 2009; Tulasi Ram et al., 2006).

Figure. 7 shows the relation between the spatial gradient of TEC and ROTI (over ASAB and DEBK) computed in the time period of 19:00-24:00 LT for geomagnetic quiet days of the year 2014. For every quiet day of the year 2014, mean of $\Delta TEC/\Delta lon$ and mean of ROTI during the time period between 19:00 LT and 24:00 LT were computed. In this time period, peak in value of TEC gradient about 2.5 TECU/deg and ROTI about 1 TECU/min were observed. To analyze the effect of

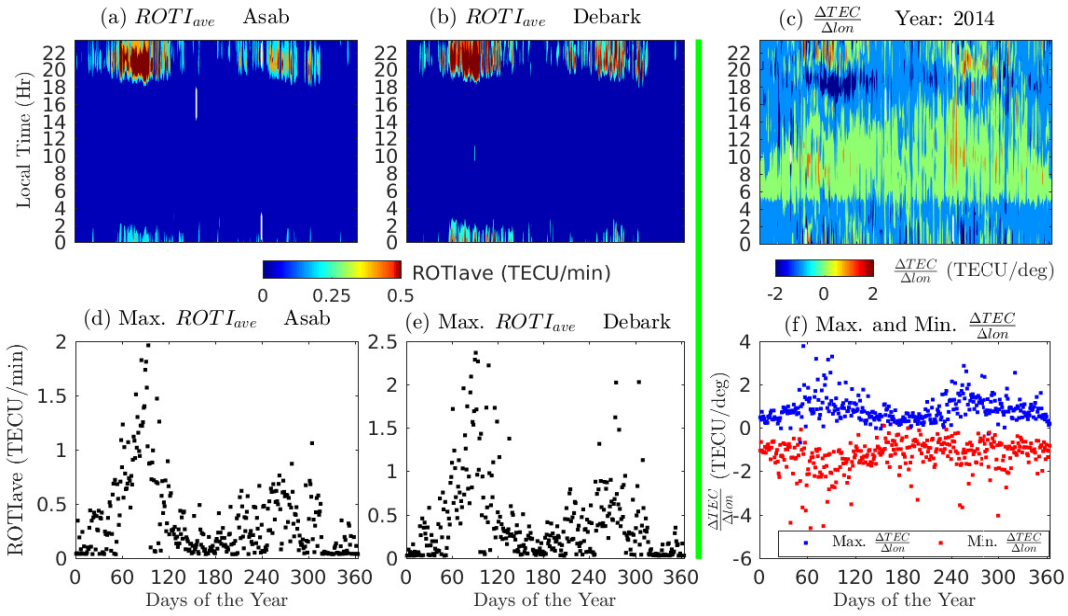

Figure 6. Ionospheric irregularity occurrence at (a) Asab (ASAB), Eritrea (b) Debark (DEBK), Ethiopia. (c) spatial gradient of TEC between ASAB and DEBK, in year 2014. Daily maximum value of $ROTI_{ave}$ (d) over ASAB, (e) over DEBK and (f) Daily maximum (blue) and minimum (red) values of spatial gradient of TEC, in year 2014. The $ROTI_{ave}$ value in TECU/min is indicated in color code.

the horizontal gradient of TEC on navigation and communication during geomagnetic storms, Radicella et al. (2004) considered the absolute value of TEC gradient. Here, we took the absolute value of the spatial gradient of TEC to describe the relationship between the TEC gradient and ROTI. The correlation coefficient between $\Delta TEC/\Delta lon$ and ROTI is about 0.58 (in ASAB) and 0.53 (in DEBK), respectively. It is well known that ROT is the combination of the spatial and temporal gradients. However, by giving less attention to the spatial gradient effect, previous authors often use $\Delta TEC/\Delta t$ to explain the TEC fluctuation determination. It is not only the temporal variation of TEC that contribute to the fluctuation in the phase and amplitude of the signals but also the spatial gradient of TEC. The computed correlation coefficient between the TEC gradient and ROTI, here, gives an indication of the contribution of the spatial gradient of TEC to ROTI (or ROT) usage. This can give the case where the spatial gradient of TEC between two nearby located stations can be used as an indicator of occurrence of ionospheric irregularities. Every night time enhancement/reduction in the gradient of TEC may not be a guarantee to indicate the occurrence/non-occurrence of ionospheric irregularities. However, there are indications which shows the occurrence of irregularities over both stations (ASAB and DEBK) when the night time enhancement/reduction in the TEC gradient were observed. By comparing the ROTI index, ionospheric TEC gradient and vertical TEC, Hua and Chunbo (2009) reported the correlation between them and their variation characteristics resulted from plasma instability in the ionosphere. Cesaroni et al. (2015) described the importance of the information provided by the TEC gradients variability and the role of the meridional TEC gradients in driving scintillation. By comparing the zonal and the meridional components of average and standard de-

viation of ΔTEC, Cesaroni et al. (2015) reported that the North-South (N-S) gradients of TEC are significantly larger than their East-West (E-W) counterparts, regardless of the season. Saito and Yoshihara (2017) associated extreme ionospheric total electron gradient with plasma bubbles for GNSS Ground-Based Augmentation System and they obtained a largest ionospheric gradient of about 3.38 TECU/km. It is suggested that when scintillation events are investigated ionospheric TEC gradient is also one of considerable parameters.

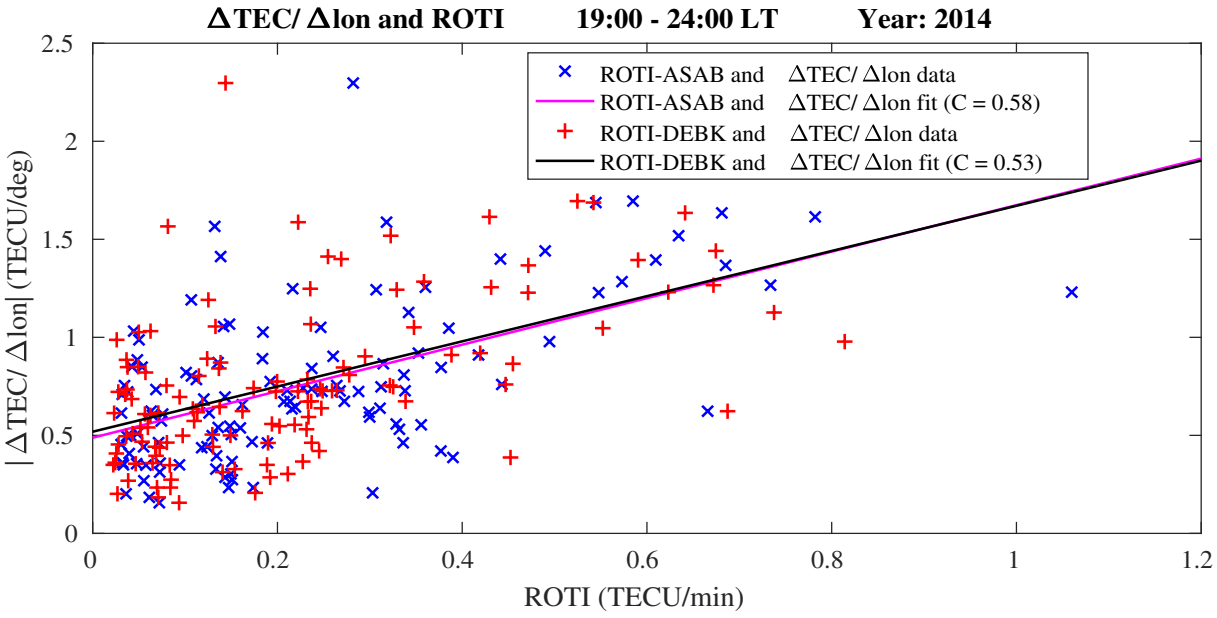

Figure 7. Relation between the spatial gradient of TEC and ROTI index derived from TEC over ASAB (blue) and DEBK (red) during 19:00-24:00 LT period of the magnetic quiet days of year 2014. The black and magenta lines indicate the linear fit between the spatial gradient of TEC and ROTI for ASAB and DEBK, respectively.

Figure 8 presents the percentage occurrence of ionospheric irregularities over ASAB (blue) and DEBK (red) in the year 2014. The observation of the percentage occurrence was made for all days of the year 2014 including both quiet and disturbed days. The percentage occurrence of irregularities was calculated by counting the number of days in a month with $ROTI_{ave} \geq 0.4$ TECU/min and dividing by the number of days in a month for which the data are available, and multiplied by 100 % (Oladipo et al., 2014). Since the two stations are close to each other, the occurrence of ionospheric irregularities observed over both stations does not show major differences. Two peaks of irregularity occurrence were observed around the middle of the equinoxes (i.e., in March and September) at both stations. This could be related to the alignment of the magnetic field lines with a geographic meridian (Burke et al., 2004; Tsunoda, 2005, 2010). The seasonal variation of ionospheric irregularities exhibits an equinoctial asymmetry in its occurrence especially at the two peaks (i.e., in March and September), where March equinox was greater than September equinox. The maximum $ROTI_{ave}$ observed over this station in the year 2014 was about 1.8 TECU/min in March 2014 and minimum level of $ROTI_{ave}$ was observed on December Solstice.

Based on a few station observations, earlier studies indicated the equinoctial asymmetry in the occurrence of L-band scintillations and they attributed to differences in the meridional winds during two equinoxes (e.g., Nishioka et al., 2008; Maruyama et al., 2006; Otsuka et al., 2006). Nishioka et al. (2008) have analyzed the occurrence characteristics of plasma bubbles using GPS-TEC obtained all over the globe and found equinoctial asymmetry in its occurrence. They have suggested that equinoctial asymmetry could be due to the asymmetric distribution of integrated conductivities during these periods. Using three ionosonde observations, Maruyama et al. (2006) reported that meridional wind is the key factor for the equinoctial asymmetry. Using multi-instrument observations, Sripathi et al. (2011) examined the equinoctial asymmetry in scintillation occurrence in the Indian sector and they suggested that the asymmetry in the electron density distribution and meridional winds as a possible causative mechanism. Manju et al. (2012) also reported equinoctial asymmetry in ESF occurrence and they discussed the possible role of asymmetric meridional winds. Manju and Haridas (2015) observed a significant asymmetry in the threshold height between the vernal equinox and autumn equinox and underlines the distinct differences in the role of neural dynamics in ESF triggering during the two equinoxes. Based on scintillation index (S_4) and GPS-TEC derived indices, the seasonal and equinoctial asymmetry in the occurrence of ionospheric irregularities over equatorial/low-latitude region of African were presented (Susnik and Forte, 2011; Paznukhov et al., 2012; Oladipo and Schuler, 2013b; Oladipo et al., 2014; Seba and Tsegaye, 2015; Mungufeni et al., 2016). By employing the horizontal wind model (HWM14), Seba et al. (2018) recently reported that the difference in the wind pattern between March and September is one of the factors for the equinoctial asymmetry. The local time and seasonal trends of occurrence of ionospheric irregularities observed in this study are similar to those reported in the previous studies (Aarons, 1993; Basu et al., 1988; Olwendo et al., 2013; Amabayo et al., 2014; Seba and Tsegaye, 2015). The equinoctial asymmetries in the occurrence of ionospheric irregularities observed in our case might also be due to the direction of the meridional winds during equinoxes over the stations.

In terms of local time, monthly, and seasonal behavior the enhancement/reduction in the spatial gradient of TEC and occurrence of ionospheric irregularities show similar trends. And, it is evident from the above result that the spatial gradient of TEC between two nearby located stations where the two receivers lie nearly along the same latitudes covey insight into the relation between large-scale ionospheric irregularity occurrence. In the current study, the optimum distance between the two GNSS receivers and the threshold value of the gradient of TEC that could indicate the occurrence of ionospheric irregularities has not been considered. This will be done in our future work.

4 Conclusions

In this study, we present for the first time the relationship between the spatial gradient of TEC between two nearby located stations (ASAB and DEBK) and the occurrence of ionospheric irregularities over Ethiopia, an equatorial region, based on GPS-TEC data. The following features were observed in the study. The daytime equatorial electrojet (EEJ) derived from H-component of geomagnetic field and the real-time electric field (EEF) model correlates linearly and positively with correlation coefficient of C = 0.6. Most of the daily maximum enhancement and/or reduction in the spatial gradient of TEC was observed in the pre-midnight and post-midnight period. In terms of seasons and months, the nighttime pattern of most of the the spatial

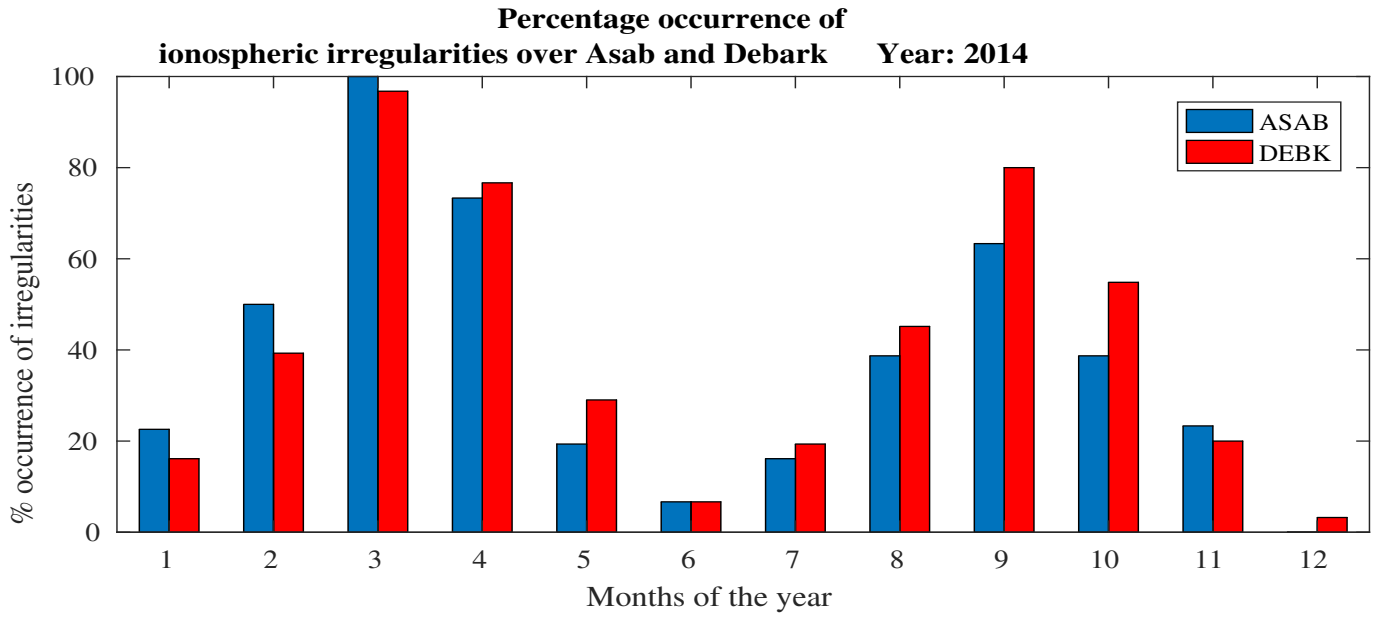

Figure 8. Percentage of occurrence of ionospheric irregularities over ASAB (red) and DEBK (blue) stations in the year 2014 based on $ROTI_{ave}$ index.

gradient of TEC and $ROTI_{ave}$ show similar trends. Both of them show maximum enhancement/reduction during the March and September months. Equinoctial asymmetry was also observed both in the spatial gradient of TEC and ROTI, where March equinox was greater than September equinox. Most of the peak values in the spatial gradient of TEC and $ROTI_{ave}$ were observed about 1-2 hrs later from post-sunset enhancement of equatorial electric field (EEF). The correlation coefficient between the magnitude of the spatial gradient of TEC and ROTI was about 0.58 (in ASAB station) and 0.53 (in DEBK station). When the occurrence of ionospheric irregularities are suppressed (for example, during geomagnetic disturbed conditions), the nighttime peak value of spatial gradient of TEC declines. Based on the above results, the spatial gradient of TEC between the two nearby located stations lying along the same geographic and geomagnetic latitudes could be associated with the presence of large-scale ionospheric irregularities. The spatial gradient of electron density (TEC) near solar-terminator obtained from two nearby located GNSS receivers method may be an alternative method to estimate the strength of the zonal electric field. The threshold value of the gradient of TEC and the minimum separation distance between stations were not presented in the current study and this will be considered in the future investigation.

Acknowledgments

We thank Ethiopian Space Science and Technology Institute (ESSTI) for facilitating conditions to do this research. We also acknowledge the administration and staff the Space Science Directorate of the South African National Space Agency (SANSA) for the support during the research visit of the first author to the institution. The authors would like to express their gratitude to

the International GNSS Service (IGS) for providing the GPS data (ftp://cddis.gsfc.nasa.gov). We thank the Cooperative Institute for Research in Environmental Sciences (CIRES) team for real-time PPEEFM model at http://geomag.org/model/PPEFM/RealtimeEF.html. We are also grateful to the online AMBER (http://magnetometers.bc.edu/index.php/) and INTERMAGNET (http://www.intermagnet.org/) for freely providing magnetometer data. Melessew Nigussie work has been supported by Air Force Office of Scientific Research, Air Force Material Command USAF under Award No.FA9550-16-1-0070. T. Dugassa, thanks Bule Hora University for permitting study leave.

Data availability

The data used in this study were obtained from ftp://cddis.gsfc.nasa.gov, http://geomag.org/models/PPEFM/RealtimeEF.html, http://magnetometers.bc.edu/index.php/, http://www.intermagnet.org/, and http://isgi.unistra.fr/data_download.php.

Competing interests

The authors declare that they have no conflict of interest.

References

Aarons, J.: The longitudinal morphology of equatorial F layer irregularities relevant to their occurrence., Space Sci. Rev., 63, 209., 1993.

Aarons, J., Mendillo, M., and Yantosca, R. G.: GPS phase fluctuations in the equatorial region during sunspot minimum., Radio Sci.., 32, 1535-1550., 1997.

Abdu, M. A., . Batista, I. S., Reinisch, B. W., de Souza, J. R., Sobral, J. H. A., Pedersen, T. R., Medeiros, A. F., Schuch, N. J., and de Paula, E. R., a. G. K. M.: Conjugate Point Equatorial Experiment (COPEX) campaign in Brazil: Electrodynamics highlights on spread development conditions and day to day variablity, J. Geophys. Res., 114, A04308, https://doi.org/10.1029/2008JA013749, 2009.

Ajith, K., Tulasi Ram, S., Yamamoto, M., Otsuka, Y., and Niranjan, K.: On the fresh development of equatorial plasma bubbles around the midnight hours of June solstice, Journal of Geophysical Research: Space Physics, 121, 9051–9062, 2016.

Amabayo, E., Jurua, E., Cilliers, P., and Habarulema, J.: Climatology of ionospheric scintillations and TEC trend over the Ugandan region. , Adv. Space Res., 53,734-743., 2014.

Anderson, D., Anghel, A., Yumoto, K., Ishitsuka, M., and Kudeki, E.: Estimating daytime vertical $E \times B$ drift velocities in the equatorial F-region using ground-based magnetometer observations, Geophys. Res. Lett., 29(12), 1596, https://doi.org/10.1029/2001GL014562, 2002.

Anderson, D., Anghel, A., Chau, J., and Veliz, O.: Daytime vertical E$\times$ B drift velocities inferred from ground-based magnetometer observations at low latitudes, Space Weather, 2, 2004.

Anderson, D., Anghel, A., Chau, J. L., and Yumoto, K.: Global, low-latitude, vertical E$\times$ B drift velocities inferred from daytime magnetometer observations, Space Weather, 4, 2006.

Arikan, F., Nayir, H., Sezen, U., and Arikan, O.: Estimation of single station interfrequency receiver bias using GPS-TEC, Radio Science, 43, 2008.

Basu, S. and Basu, S.: Equatorial scintillations-A review, Journal of Atmospheric and Terrestrial Physics, 43, 473–489, 1981.

Basu, S., MacKenzie, E., and Basu, S.: Ionospheric constraints on VHF/UHF communications links during solar maximum and minimum periods, Radio Science, 23, 363–378, 1988.

Basu, S., Kudeki, E., Basu, S., Valladares, C., Weber, E., Zengingonul, H., Bhattacharyya, S., Sheehan, R., Meriwether, J., Biondi, M., Kuenzler, H., and Espinoza, J.: Scintillations, plasma drifts, and neutral winds in the equatorial ionosphere after sunset, J. Geophys Res, 101, 26795-26809, 1996.

Batista, I., Abdu, M., and Bittencourt, J.: Equatorial F region vertical plasma drifts: Seasonal and longitudinal asymmetries in the American sector, Journal of Geophysical Research: Space Physics, 91, 12 055–12 064, 1986.

Bhattacharyya, A., Beach, T., Basu, S., and Kintner, P.: Nighttime equatorial ionosphere: GPS scintillations and differential carrier phase fluctuations, Radio Science, 35, 209–224, 2000.

Bolaji, O., Adebiyi, S., and Fashae, J.: Characterization of ionospheric irregularities at different longitudes during quiet and disturbed geomagnetic conditions, Journal of Atmospheric and Solar-Terrestrial Physics, 182, 93–100, 2019.

Burke, W. J., Gentile, L. C., Huang, C. Y., Valladares, C. E., and Su, S. Y.: Longitudinal variability of equatorial plasma bubbles observed by DMSP and ROCSAT-1, J. Geophys. Res., 19, https://doi.org/10.1029/2004JA010583, 2004.

Cesaroni, C., Spogli, L., Alfonsi, L., De Franceschi, G., Ciraolo, L., Monico, J. F. G., Scotto, C., Romano, V., Aquino, M., and Bougard, B.: L-band scintillations and calibrated total electron content gradients over Brazil during the last solar maximum, Journal of Space Weather and Space Climate, 5, A36, 2015.

Chu, F., Liu, J.Y., a. T. H., Sobral, J., Taylor, M., and Medeiros, A. F.: The climatology of ionospheric plasma bubbles and irregularities over Brazil, Annales Geophysical, 23: 379-384, 2005.

Crain, D., Heelis, R., and Bailey, G.: Effects of electrical coupling on equatorial ionospheric plasma motions: When is the F region a dominant driver in the low-latitude dynamo?, Journal of Geophysical Research: Space Physics, 98, 6033–6037, 1993.

Dabas, R., Singh, L., Lakshmi, D., Subramanyam, P., Chopra, P., and Garg, S.: Evolution and dynamics of equatorial plasma bubbles: Relationships to ExB drift, postsunset total electron content enhancements, and equatorial electrojet strength, Radio Science, 38, 2003.

Dugassa, T., Habarulema, J. B., and Nigussie, M.: Longitudinal variability of occurrence of ionospheric irregularities over the American, African and Indian regions during geomagnetic storms, Advances in Space Research, 2019.

Echer, E., Tsurutani, B., and Gonzalez, W.: Interplanetary origins of moderate (- 100 nT< Dst- 50 nT) geomagnetic storms during solar cycle 23 (1996–2008), Journal of Geophysical Research: Space Physics, 118, 385–392, 2013.

Farley, D., Balsey, B., Woodman, R., and McClure, J.: Equatorial spread F: Implications of VHF radar observations, Journal of Geophysical Research, 75, 7199–7216, 1970.

Farley, D. T., Bonelli, E., Fejer, B. G., and Larsen, M. F.: The prereversal enhancement of the zonal electric field in the equatorial ionosphere., J. Geophys. Res., 113,A05304., 2008.

Fejer, B.: Low latitude electrodynamics plasma drifts: a review., J. Atmos. Terr. Phys., 53, 677-693, 1991.

Fejer, B., Jensen, J., and Su, S.: Quiet time equatorial F region vertical plasma drift model derived from ROCSAT-1 observations., J. Geophys. Res., https://doi.org/http://dx.doi.org/10.1029/2007JA012801., 2008.

Fejer, B. G., Scherliess, L., and de Paula, E. R.: Effects of the vertical plasma drift velocity on the generation and evolution of equatorial spread F, J. Geophys. Res., 104, 19,859-19,869, https://doi.org/10.1029/1999JA900271, 1999.

Foster, J.: Quantitative investigation of ionospheric density gradients at mid latitudes, in: Proceedings of the Institute of Navigation ION 2000 Conference, 2000.

Hajra, R., Chakraborty, S., Mazumdar, S., and Alex, S.: Evolution of equatorial irregularities under varying electrodynamical conditions: a multitechnique case study from Indian longitude zone, Journal of Geophysical Research: Space Physics, 117, 2012.

Heelis, R., Kendall, P., Moffett, R., Windle, D., and Rishbeth, H.: Electrical coupling of the E-and F-regions and its effect on F-region drifts and winds, Planetary and Space Science, 22, 743–756, 1974.

Hua, H. W. C. Y. S. and Chunbo, Z.: Study of Ionospheric TEC Horizontal Gradient by Means of GPS Observations [J], Chinese Journal of Space Science, 2, 2009.

Jakowski, N., Leitinger, R., and Ciraolo, L.: Behaviour of large scale structures of the electron content as a key parameterfor range errors in GNSS applications, Annals of Geophysics, 47, 2004.

Jakowski, N., Stankov, S., and Klaehn, D.: Operational space weather service for GNSS precise positioning, in: Annales Geophysicae, vol. 23, pp. 3071–3079, 2005.

Kassa, T. and Damtie, B.: Ionospheric irregularities over Bahir Dar, Ethiopia during selected geomagnetic storms, Advances in Space Research, 60, 121–129, 2017.

Kelley, M. C.: The Earth's ionosphere: plasma physics and electrodynamics, vol. 96, Academic press, 2009.

Lee, J., Pullen, S., Datta-Barua, S., and Enge, P.: Assessment of ionosphere spatial decorrelation for global positioning system-based aircraft landing systems, Journal of Aircraft, 44, 1662–1669, 2007.

Lee, J. H., Pullen, S., Datta-Barua, S., and Enge, P.: Assessment of nominal ionosphere spatial decorrelation for laas, in: 2006 IEEE/ION Position, Location, And Navigation Symposium, 2010.

Loewe, C. A. and Prölss, G. W.: Classification and mean behavior of magnetic storms, Journal of Geophysical Research: Space Physics, 102, 14 209–14 213, 1997.

Ma, G. and Maruyama, T.: Derivation of TEC and estimation of instrumental biases from GEONET in Japan, in: Annales Geophysicae, vol. 21, pp. 2083–2093, 2003.

Ma, G. and Maruyama, T.: A super bubble detected by dense GPS network at East Asian longitudes., Geophys. Res. Lett., 133, L21103, 2006.

Magdaleno, S., Herraiz, M., Altadill, D., and Benito, A.: Climatology characterization of equatorial plasma bubbles using GPS data, Journal of Space Weather and Space Climate, 7, A3, 2017.

Manju, G. and Haridas, M. M.: On the equinoctial asymmetry in the threshold height for the occurrence of equatorial spread F, Journal of Atmospheric and Solar-Terrestrial Physics, 124, 59–62, 2015.

Manju, G., Devasia, C., and Ravindran, S.: The seasonal and solar cycle variations of electron density gradient scale length, vertical drift and layer height during magnetically quiet days: Implications for Spread F over Trivandrum, India, Earth, planets and space, 61, 1339–1343, 2009.

Manju, G., Haridas, M., Ravindran, S., Pant, T. K., and Ram, S. T.: Equinoctial asymmetry in the occurrence of equatorial spread-F over Indian longitudes during moderate to low solar activity period 2004-2007, 94.20. dt; 94.20. Vv; 96.60. qd, 2012.

Manoj, C. and Maus, S.: A real-time forecast service for the ionospheric equatorial zonal electric field., Space Weather, 10, https://doi.org/http://dx.doi.org/10.1029/2012SW00082, 2012.

Martinis, C. R., Mendillo, M. J., and Aarons, J.: Toward a synthesis of equatorial spread F onset and suppression during geomagnetic storms, J. Geophys. Res., 110, A07306, https://doi.org/10.1029/2003JA010362, 2005.

Maruyama, T., Saito, S., Kawamura, M., Nozaki, K., Krall, J., and D.Huba, J.: Equinoctial asymmetry of a low-latitude ionosphere-thermosphere system and equatorial irregularities: Evidence for meridional wind control., Ann. Geophys., 27, 2027-2034, https://doi.org/10.5194/angeo-27-2027-2009, 2006.

Mendillo, M., Lin, B., and Aarons, J.: The application of GPS observations to equatorial aeronomy., Radio Sci., 35, 885-904., 2000.

Mendillo, M., Meriwether, J., and Biondi, M.: Testing the thermospheric neutral wind suppression mechanism for day-to-day variability of equatorial spread F., J. Geophys. Res., 106, 3655., 2001.

Muella, M., De Paula, E., Kantor, I., Batista, I., Sobral, J., Abdu, M., Kintner, P., Groves, K., and Smorigo, P.: GPS L-band scintillations and ionospheric irregularity zonal drifts inferred at equatorial and low-latitude regions, Journal of Atmospheric and Solar-Terrestrial Physics, 70, 1261–1272, 2008.

Mungufeni, P., Jurua, E., and Habarulema, J.: Trends of ionospheric irregularities over African low latitude region during quiet geomagnetic conditions., J. Atmos. Solar Terr. Phys., 138-139, 261-267, https://doi.org/http://dx.doi.org/10.1016/j.jastp.2016.01.015, 2016.

Mushini, S. C., P. T. J. R. B. L. J. W. M. and Pokhotelov, D.: Improved amplitude and phase scintillation indices derived from wavelet detrended high latitude GPS data, PS Solut., https://doi.org/10.1007/s10291-011-0238-4, 2011.

Nava, B., Radicella, S., Leitinger, R., and Coïsson, P.: Use of total electron content data to analyze ionosphere electron density gradients, Advances in Space Research, 39, 1292–1297, 2007.

Nayak, C., Tsai, L.-C., Su, S.-Y., Galkin, I., Caton, R., and Groves, K.: Suppression of ionospheric scintillation during St. Patrick's Day geomagnetic super storm as observed over the anomaly crest region station Pingtung, Taiwan: A case study, Advances in Space Research, 60, 396-405, https://doi.org/http://dx.doi.org/10.1016/j.asr.2016.11.036, 2017.

Nishioka, M., Saito, A., and Tsugawa, T.: Occurrence characteristics of plasma bubble derived from global ground-based GPS receiver networks, J. Geophys. Res., 113, A05301, https://doi.org/10.1029/2007JA012605, 2008.

Oladipo, O. A. and Schuler, T.: Magnetic storm effect on the occurrence of ionospheric irregularities at an equatorial station in the African sector, Ann.Geophys., 56, 5, A0565, https://doi.org/10.4401/ag-6247, 2013a.

Oladipo, O. A. and Schuler, T.: Equatorial ionospheric irregularities using GPS TEC derived index., Atmos. Sol. Terr. Phys., 92, 78-82., 2013b.

Oladipo, O. A., Adeniyi, J. O., Olawepo, A. O., and Doherty, P. H.: Large-scale ionospheric irregularities occurrence at Ilorin, Nigeria, Space Weather., 12, 300-305., https://doi.org/10.1002/2013SW000991, 2014.

Olwendo, J., Cilliers, P., Weimin, Z., Ming, O., and Yu, X.: Validation of ROTI index for ionospheric amplitude scintillation measurements in a low latitude region over Africa., Radio Science, 2018.

Olwendo, O., Baluku, T., Baki, P., Cilliers, P., Mito, C., and Doherty, P.: Low latitude ionospheric scintillation and zonal irregularity drifts observed with GPS-SCINDA system and closely spaced VHF receivers in Kenya, Adv. in Space Res., 51, 1715-1726., https://doi.org/http://dx.doi.org/10.1016/j.asr.2012.12.017, 2013.

Otsuka, Y., Shiokawa, K., and Ogawa, T.: Equatorial ionospheric scintillations and zonal irregularity drifts observed with closely spaced GPS receivers in Indonesia., J. Meteorol. Soc. Jpn., 84A, 343-351, 2006.

Otsuka, Y., Ogawa, T., et al.: VHF radar observations of nighttime F-region field-aligned irregularities over Kototabang, Indonesia, Earth, planets and space, 61, 431–437, 2009.

Paznukhov, V., Carrano, C., Doherty, P., Groves, K., Caton, R.G., a. V. C., Seemala, G., Bridgwood, C., Adeniyi, J., Amaeshi, L., Damtie, B., a. D. M. F., Ndeda, J., Baki, P., Obrou, O., Okere, B., and Tsidu, G.: Equatorial plasma bubbles and L-band scintillations in Africa during solar minimum., Ann. Geophys., 30, 675-682, 2012.

Pi, X., Mannucci, A. J., Lindqdwister, U. J., and Ho, C.: Monitoring of Global Ionospheric Irregularities using the worldwide GPS, Geophys. Res. Lett., 24, 2283-2286, https://doi.org/10.1029/97GL02273, 1997.

Pradipta, R. and Doherty, P. H.: Assessing the occurrence pattern of large ionospheric TEC gradients over the Brazilian airspace, Navigation: Journal of The Institute of Navigation, 63, 335–343, 2016.

Radicella, S. M., Nava, B., Coïsson, P., Kersley, L., and Bailey, G. J.: Effects of gradients of the electron density on Earth-space communications, Annals of Geophysics, 47, 2004.

Ram, S. T., Rao, P. R., Prasad, D., Niranjan, K., Babu, A. R., Sridharan, R., Devasia, C., and Ravindran, S.: The combined effects of electrojet strength and the geomagnetic activity (Kp-index) on the post sunset height rise of the F-layer and its role in the generation of ESF during high and low solar activity periods, Ann. Geophys, 25, 2007.

Rao, P. R., Krishna, S. G., Niranjan, K., and Prasad, D.: Study of spatial and temporal characteristics of L-band scintillations over the Indian low-latitude region and their possible effects on GPS navigation, in: Annales Geophysicae, vol. 24, pp. 1567–1580, 2006a.

Rao, P. R., Krishna, S. G., Niranjan, K., and Prasad, D.: Temporal and spatial variations in TEC using simultaneous measurements from the Indian GPS network of receivers during the low solar activity period of 2004-2005, in: Annales Geophysicae, vol. 24, pp. 3279–3292, 2006b.

Rastogi, R. and Woodman, R.: Spread F in equatorial ionograms associated with reversal of horizontal F region electric field, in: Annales de Geophysique, vol. 34, pp. 31–36, 1978.

Rastogi, R., Kitamura, T., and Kitamura, K.: Geomagnetic field variations at the equatorial electrojet station in Sri Lanka, Peredinia, in: Annales Geophysicae, vol. 22, pp. 2729–2739, 2004.

Rastogi, R. G. and Klobuchar, J. A.: Ionospheric electron content within the equatorial F2 layer anomaly belt., J. Geophys. Res, 95(A11),19,045-19,052, 1990.

Ratnam, D. V., Vishnu, T. R., and Harsha, P. B. S.: Ionospheric Gradients Estimation and Analysis of S-Band Navigation Signals for NAVIC System, IEEE Access, 6, 66 954–66 962, 2018.

Ravi Chandra, K., Satya Srinivas, V., and Sarma, A.: Investigation of ionospheric gradients for GAGAN application, Earth, planets and space, 61, 633–635, 2009.

Ray, S., Paul, A., and Dasgupta, A.: Equatorial scintillations in relation to the development of ionization anomaly, in: Annales Geophysicae, vol. 24, pp. 1429–1442, 2006.

Rungraengwajiake, S., Supnithi, P., Saito, S., Siansawasdi, N., and Saekow, A.: Ionospheric delay gradient monitoring for GBAS by GPS stations near Suvarnabhumi airport, Thailand, Radio Science, 50, 1076–1085, 2015.

Saito, S. and Yoshihara, T.: Evaluation of extreme ionospheric total electron content gradient associated with plasma bubbles for GNSS Ground-Based Augmentation System, Radio Science, 52, 951-962, 2017.

Sardón, E. and Zarraoa, N.: Estimation of total electron content using GPS data: How stable are the differential satellite and receiver instrumental biases?, Radio science, 32, 1899–1910, 1997.

Seba, E. and Nigussie, M.: Investigating the effect of geomagnetic storm and equatorial electrojet on equatorial ionospheric irregularity over East African sector., Adv. Space Res., 58,1708–1719, 2016.

Seba, E. and Tsegaye, K. G.: Characterization of ionospheric scintillation at a geomagnetic equatorial region station., Adv. Space Res., 56, 2057-2063, 2015.

Seba, E. B., Nigussie, M., and Moldwin, M. B.: The relationship between equatorial ionization anomaly and nighttime equatorial spread F in East Africa, Advances in Space Research, 62, 1737–1752, 2018.

Seemala, G. and Valladares, C.: Statistics of total electron content depletions observed over the South American continent for the year 2008, Radio Science, 46, RS5019, 2011.

Sreeja, V., Devasia, C., Ravindran, S., and Pant, T. K.: Observational evidence for the plausible linkage of Equatorial Electrojet (EEJ) electric field variations with the post sunset F-region electrodynamics, in: Annales geophysicae: atmospheres, hydrospheres and space sciences, vol. 27, p. 4229, 2009.

Sripathi, S., Kakad, B., and Bhattacharyya, A.: Study of equinoctial asymmetry in the Equatorial Spread F (ESF) irregularities over Indian region using multi-instrument observations in the descending phase of solar cycle 23, J. Geophys. Res., 116, A11302, https://doi.org/10.1029/2011JA016625., 2011.

Sun, Y.-Y., Matsuo, T., Araujo-Pradere, E. A., and Liu, J.-Y.: Ground-based GPS observation of SED-associated irregularities over CONUS, Journal of Geophysical Research: Space Physics, 118, 2478–2489, 2013.

Susnik, A. and Forte, B.: Ionospheric scitillation activity measured in the African sector, paper presented at General Assembly and Scientific Symposium, XXXth URSI, Istanbul, Turkey., 2011.

Takahashi, H., Wrasse, C., Denardini, C., Pádua, M., de Paula, E., Costa, S., Otsuka, Y., Shiokawa, K., Monico, J. G., Ivo, A., et al.: Ionospheric TEC weather map over South America, Space Weather, 14, 937–949, 2016.

Tsunoda, R.: Control of the seasonal and longitudinal occurrence of equatorial scintillations by the longitudinal gradient in integrated E region Pederson conductivity., J. Geophys. Res., 90, 447., 1985.

Tsunoda, R. T.: On the enigma of day-to-day variability in Wave structure in equatorial Spread F, Geophys. Res. Lett., 32, 2005.

Tsunoda, R. T.: On seeding equatorial spread F during solstices, Geophys. Res. Lett., 37, L05102., https://doi.org/http://dx.doi.org/10.1029/2010GL042576., 2010.

Tulasi Ram, S., Rao, P. V. S. R., Niranjan, K., Prasad, D. S. V. V. D., Sridharan, R., Devasia, C. V., and Ravindran, S.: The role of post-sunset vertical drifts at the equator in predicting the onset of VHF scintillations during high and low sunspot activity years., Ann. Geophys., 24, 1609-1616, 2006.

Uemoto, J., Maruyama, T., Saito, S., Ishii, M., and Yoshimura, R.: Relationships between pre-sunset electrojet strength, pre-reversal enhancement and equatorial spread-F onset., Annales Geophysicae (09927689), 28, 2010.

Valladares, C., Basu, S., Groves, K., Hagan, M., Hysell, D., Mazzella Jr., A., and Sheehan, R.: Measurement of the latitudinal distribution of total electron content during equatorial spread-F events, J. Geophys. Res., 106, 29133-29152, 2001.

Valladares, C., Villalobos, J., Sheehan, R., and Hagan, M.: Latitudinal extension of low-latitude scintillations measured with a network of GPS receivers, Ann. Geophys., 22, 3155-3175, 2004.

Watthanasangmechai, K., Yamamoto, M., Saito, A., Tsunoda, R., Yokoyama, T., Supnithi, P., Ishii, M., and Yatini, C.: Predawn plasma bubble cluster observed in Southeast Asia, Journal of Geophysical Research: Space Physics, 121, 5868–5879, 2016.

Wernik, A. and Liu, C.: Ionospheric irregularities causing scintillation of GHz frequency radio signals, Journal of Atmospheric and Terrestrial Physics, 36, 871–879, 1974.

Wiens, R. H., Ledvina, B. M., a. K. P. M., Afewerki, M., and Mulugheta, Z.: Equatorial plasma bubbles in the ionosphere over Eritrea: Occurrence and drift speed, Ann. Geophys.,, 24, 1443–1453, 2006.

Woodman, R.: Vertical drift velocities and East-West electric fields at the magnetic equator., J. Geophys. Res., 75(31), 6249-6259, https://doi.org/10.1029/JA075i031p06249, 1970.

Yizengaw, E. and Moldwin, M. B.: African Meridian B-field Education and Research (AMBER) array., Earth Moon Planet, 104, 237-246, https://doi.org/10.1007/s11038-008-9287-2, 2009.

Yizengaw, E., Moldwin, M. B., Mebrahtu, A., Damtie, B., Zesta, E., Valladares, C. E., and Doherty, P.: Comparison of storm time equatorial ionospheric electrodynamics in the African and American sectors, J. Atmos. Sol.-Terr. Phys., 73(1), 156–163, https://doi.org/10.1016/j.jastp.2010.08.008., 2011.

Yizengaw, E., Zesta, E., a. M. M. B., Damtie, B., Mebrahtu, A., Valladares, C. E., and Pfaff, R. F.: Longitudinal differences of ionospheric vertical density distribution and equatorial electrodynamics., J. Geophys. Res., 117, A07312, https://doi.org/10.1029/2011JA017454., 2012.

Yizengaw, E., Moldwin, M. B., Zesta, E.and Biouele, C. M., Damtie, B., Mebrahtu, A., Rabiu, B., Valladares, C. F., and Stoneback, R.: The longitudinal variability of equatorial electrojet and vertical drift velocity in the African and American sectors., Ann. Geophys., 32, 231-238, 2014.

Yoshihara, T., Sakai, T., Fujii, N., and Saitoh, A.: An investigation of local-scale spatial gradient of ionospheric delay using the nation-wide GPS network data in Japan, in: ION National Technical Meeting, San Diego, CA, 2005.